Article

Current Biology

Evolutionarily conserved aspects of animal nutrient uptake and transport in sea anemone vitellogenesis

Graphical abstract

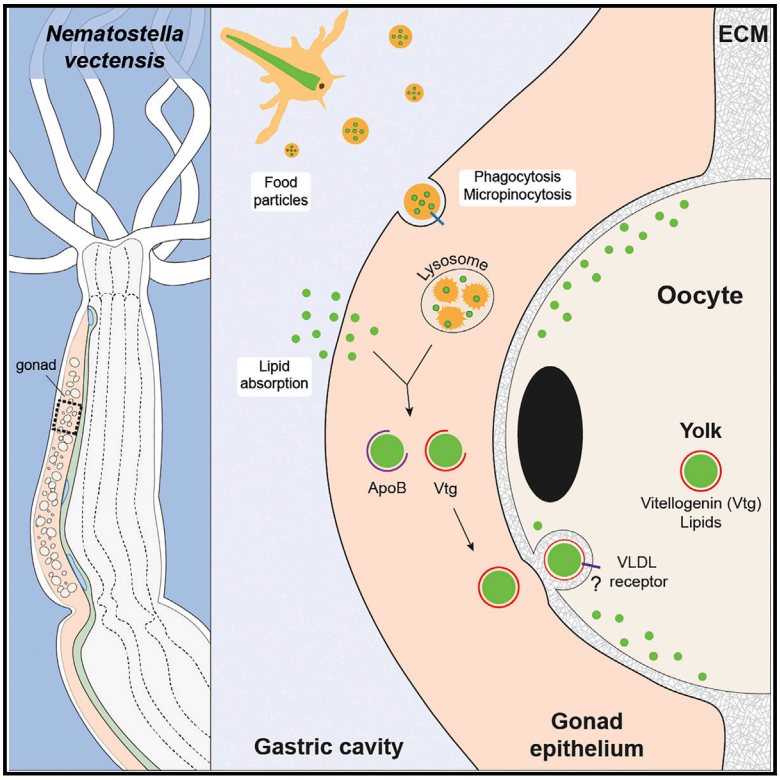

Highlights

- *Nematostella* somatic gonad epithelium shows high levels of endocytosis
- Fatty acids rapidly translocate through the gonad epithelium and ECM into oocytes
- Conserved *vitellogenin/vldlr* pair likely mediates vitellogenic lipid transport
- ECM-based yolk precursor transport may predate cnidarian-bilaterian split

Authors

Marion Lebouvier,
Paula Miramón-Puértolas,
Patrick R.H. Steinmetz

Correspondence

patrick.steinmetz@uib.no

In brief

In the sea anemone *Nematostella vectensis*, the *vitellogenin-/apoB*-expressing gonad epithelium exhibits high endocytosis and fatty acid translocation levels during vitellogenesis. Complementary expression of *vldl receptor* genes in oocytes supports that ECM-based lipoprotein transport is evolutionarily conserved between cnidarians and bilaterians.

Lebouvier et al., 2022, Current Biology *32*, 4620–4630
November 7, 2022
https://doi.org/10.1016/j.cub.2022.08.039

CellPress

CellPress
OPEN ACCESS

Current Biology

Article

Evolutionarily conserved aspects of animal nutrient uptake and transport in sea anemone vitellogenesis

Marion Lebouvier,[1] Paula Miramón-Puértolas,[1] and Patrick R.H. Steinmetz[1,2,3,*]
[1]Sars International Centre for Marine Molecular Biology, University of Bergen, Thormøhlensgate 55, 5008 Bergen, Norway
[2]Twitter: @PRHSteinmetz
[3]Lead contact
*Correspondence: patrick.steinmetz@uib.no
https://doi.org/10.1016/j.cub.2022.08.039

SUMMARY

The emergence of systemic nutrient transport was a key challenge during animal evolution, yet it is poorly understood. Circulatory systems distribute nutrients in many bilaterians (e.g., vertebrates and arthropods) but are absent in non-bilaterians (e.g., cnidarians and sponges), where nutrient absorption and transport remain little explored at molecular and cellular levels. Vitellogenesis, the accumulation of egg yolk, necessitates high nutrient influx into oocytes and is present throughout animal phyla and therefore represents a well-suited paradigm to study nutrient transport evolution. With that aim, we investigated dietary nutrient transport to the oocytes in the cnidarian *Nematostella vectensis* (Anthozoa). Using a combination of fluorescent bead labeling and marker gene expression, we found that phagocytosis, micropinocytosis, and intracellular digestion of food components occur within the gonad epithelium. Pulse-chase experiments further show that labelled fatty acids rapidly translocate from the gonad epithelium through the extracellular matrix (ECM) into oocytes. Expression of conserved lipid transport proteins *vitellogenin* (*vtg*) and *apolipoprotein-B* (*apoB*) and colocalization of labeled fatty acids with a fluorescently tagged ApoB protein further support the lipid-shuttling role of the gonad epithelium. Complementary oocyte expression of *very low-density lipoprotein receptor* (*vldlr*) orthologs, which mediate endocytosis of bilaterian ApoB- and Vtg-lipoproteins, supports that this evolutionarily conserved ligand/receptor pair underlies lipid transport during sea anemone vitellogenesis. In addition, we identified lipid- and ApoB-rich cells with potential lipid transport roles in the ECM. Altogether, our work supports a long-standing hypothesis that an ECM-based lipid transport system predated the cnidarian-bilaterian split and provided a basis for the evolution of bilaterian circulatory systems.

INTRODUCTION

The emergence of circulatory systems ensured a constant nutrient supply to all tissues during the evolution of large and complex body plans in many bilaterians.[1,2] Non-bilaterians, in contrast, exhibit much simpler body plans that lack circulatory systems and consist of mostly two cell layers without intermediate tissues. It is therefore widely assumed that systemic nutrient distribution by circulatory systems has emerged in bilaterian lineages.[1–3] As dietary nutrient uptake and transport are poorly studied on a cellular or molecular level in any non-bilaterian animal, the evolutionary origin of animal nutrient transport systems remains speculative. A prevailing hypothesis proposes that fluid and nutrient transport through an increasingly porous extracellular matrix (ECM), as reflected by blood vascular system development in many bilaterians, represents the ancestral condition from which bilaterian circulatory systems have further specialized.[1–3] Here, we test this hypothesis by investigating whether ECM-based nutrient uptake and transport mechanisms are conserved between cnidarian and bilaterian vitellogenesis.

Yolk production necessitates large amounts of nutrients, especially lipids and proteins, and is one of the most widely studied nutrient transport processes in bilaterians.[4] Vitellogenin (Vtg) and ApolipoproteinB (ApoB; Apolipophorins in insects), two proteins of the large lipid transfer protein (LLTP) superfamily, play conserved roles during bilaterian lipid transport.[5,6] Vtg is an egg yolk precursor protein that is primarily produced in female extra-ovarian tissues (e.g., vertebrate liver, insect fat body) and mediates lipid transport specifically into oocytes.[4,7–9] ApoB, in contrast, shuttles lipids systemically between the gut epithelium, vitellogenic organs, and other peripheral tissues.[10–12] In many bilaterians, Vtg and ApoB lipoproteins move through hemolymph or blood vascular systems[4] and are endocytosed into oocytes or other target tissues (e.g., muscles) by conserved orthologs of the very low-density lipoprotein (VLDL) receptor family (including arthropod Vtg or Apolipophorin receptors).[13–15] Although Vtg or ApoB orthologs are almost ubiquitously present among animal phyla,[16–18] their role in systemic lipoprotein transport is poorly studied in many animals, especially non-bilaterians.

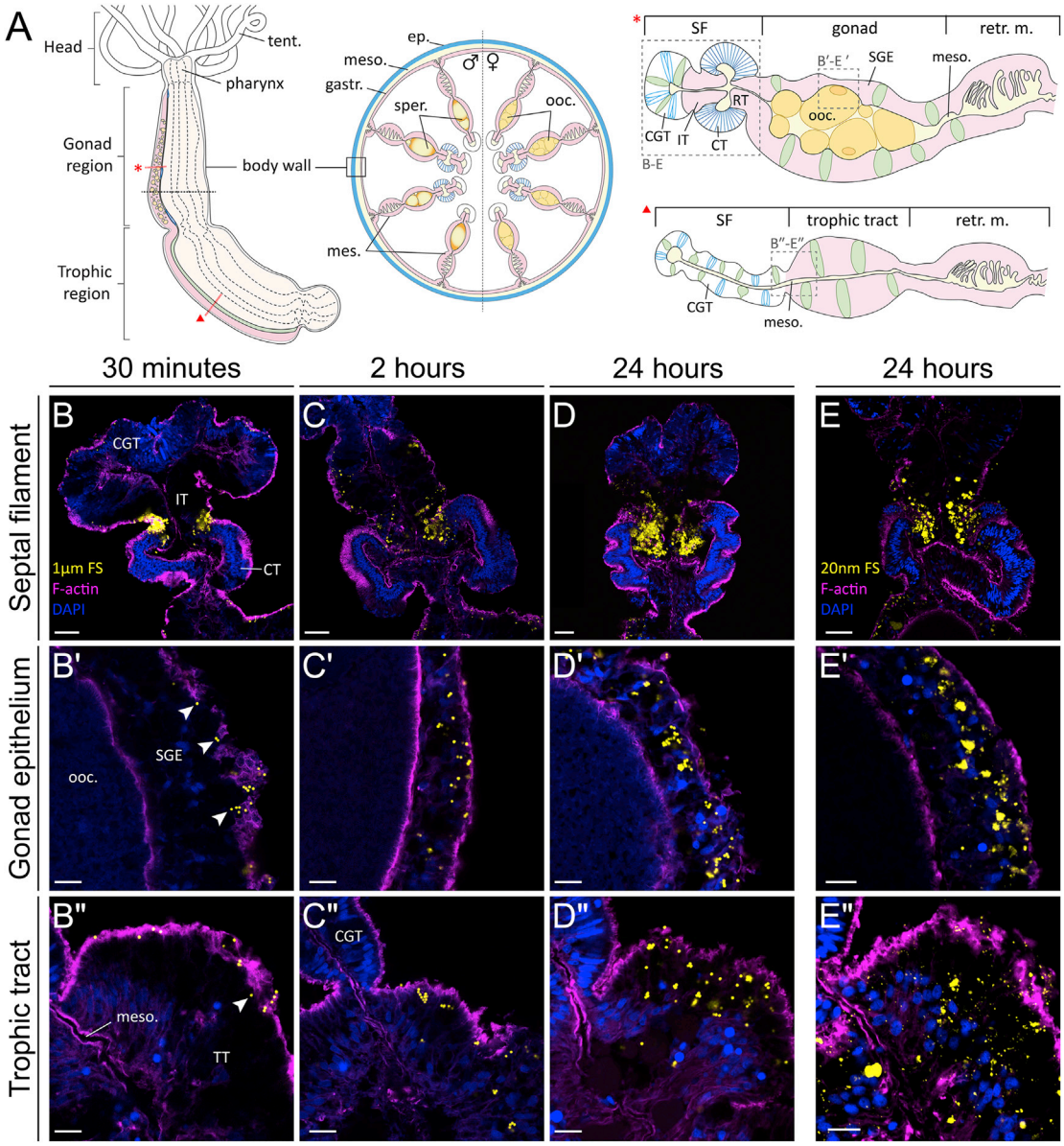

Figure 1. Regionally specific uptake of 1 μm and 20 nm FluoSpheres (FS) by the mesenterial epithelium

(A) Schematic representation of *Nematostella* morphology.

(B–E″) Uptake of 1 μm (B–D″) or 20 nm (E–E″) FluoSpheres (yellow) by specific parts of the mesenteries. 1 μm FS are progressively internalized into cells of the intermediate tract (IT) (B–E), gonad epithelium (B′–E′), and trophic tract (B″–E″) after 30 min (B–B″), 2 h (C–C″), and 24 h (D–D″) of incubation. A similar distribution of particle uptake is seen when incubating with 20 nm FS (E–E″). Distal end of mesenteries oriented to the top (B–E″).

All data figures represent single confocal plane images of adult *Nematostella* mesentery cross sections. Arrowheads in (B′) and (B″): intracellular beads as estimated by their relative location to cortical F-actin enrichment. Magenta, phalloidin (F-actin); blue, DAPI. Scale bars, 25 μm (B–E) and 10 μm (E′ and E″). CGT, cnidoglandular tract; CT, ciliated tract; ep, epidermis; gastr, gastrodermis; IT, intermediate tract; mes, mesentery; meso, mesoglea; ooc, oocyte; retr. m, retractor muscle; SGE, somatic gonad epithelium; SF, septal filament; tent, tentacle; TT, trophic tract.

See also Figure S1.

The sea anemone *Nematostella vectensis* exhibits a typical cnidarian body plan consisting of only two epithelia: the inner gastrodermis and outer epidermis. Food uptake occurs through the mouth into the blind-ended gastric cavity. As gastrodermal cilia create internal fluid flows, the gastric cavity is commonly thought to constitute the main nutrient distribution system in this phylum.[19] Gastrodermal folds (mesenteries) reach into the gastric cavity and likely represent an ancestral feature of cnidarians.[20,21] They are subdivided into functionally distinct regions such as the gonad[22–24] (Figure 1A). Oocytes or spermaries locate to mesenteries within the oral half of the *Nematostella* body column (Figure 1A, "gonad region"). Here, they are embedded in the ECM, the mesoglea, between two layers of somatic gonad epithelia[24,25] (Figure 1A). Their mesogleal localization, isolated

from direct food access, is common among anthozoans (sea anemones, corals, sea pens), scyphozoans ("true" jellies), cubozoans (cube jellies), and hydrozoan medusae[19,26] and thus likely ancestral among cnidarians. This raises the question of whether nutrients reach the cnidarian oocytes via the ECM using molecules and mechanisms that are evolutionarily conserved between cnidarians and bilaterians.

Here, we have investigated how nutrients, especially lipids, are transported from the gastric cavity to the oocyte in *Nematostella* to better understand the evolution of animal dietary lipid transport systems. The comparison with well-studied bilaterians, the phylogenetic sister group to cnidarians, has allowed the reconstruction of key cellular and molecular aspects of the lipid transport system present in the last common ancestors of cnidarians and bilaterians.

RESULTS

High endocytic activities are restricted to specialized regions of the *Nematostella* mesentery

The body regions absorbing food particles or nutrients are only vaguely described in sea anemones[27–29] and are currently unknown in *Nematostella*. We therefore used 1 μm and 20 nm bovine serum albumin (BSA)-coated fluorescent microspheres (FS, FluoSpheres) to probe for phagocytosis or micropinocytosis, respectively, in adult *Nematostella* polyps[30–32] (Figures 1B–1E″ and S1). We found that 20 nm beads, but not the 1 μm beads, were enriched in the body wall epidermis after 24 h of incubation (Figures S1A and S1B). This result suggests that micropinocytosis of nano-sized particles from the surrounding water is the principal absorptive mechanism of the outer epithelium. Both bead sizes were present in the gastrodermis of the body wall and were strongly enriched in tentacles (Figures S1C and S1D) and in three different parts of the mesenteries: the intermediate tract (IT) (Figures 1A–1E), the somatic gonad epithelium (SGE) (Figures 1A and 1B′–1E′), and the trophic tract (TT) (Figures 1A and 1B″–1E″). In contrast, all other mesentery regions remain largely devoid of beads (Figures 1A–1E″). Notably, we have not observed any bead uptake into trophonema cells (n = 11 trophonemata with 20 nm FS, n = 14 trophonemata with 1 μm FS; asterisks in Figures S1E and S1F). Phagocytosis of 1 μm FS becomes apparent after 30 min of incubation (Figures 1B–1B″) and leads to intracellular accumulation after 2 and 24 h (Figures 1C–1D″). A similar uptake distribution is observed using fluorescently labeled, heat-killed *E. coli* cells, confirming the physiological relevance of BSA-coated bead experiments (Figures S1G–S1G″).

Interested to explore whether endocytosed microspheres become mobilized, we used a 4-h incubation pulse of 20 nm beads and found similar distributions after 20-h-, 7-day-, and 14-day-long chase periods (Figures S1H–S1K″), indicating that no transport occurs between body regions. Biweekly incubations over 2 weeks led to an intracellular accumulation of 20 nm beads in the apical half of SGE cells (Figures S1L and S1M). Notably, a subset of SGE cells, which due to their abundance in the SGE are likely mucus cells,[33] shows no nanobead uptake (Figures S1L and S1M). We found altogether that three mesenterial regions, including the SGE, show increased phago- and micropinocytosis activities in *Nematostella*.

Phagocytic cell types are well studied on the molecular level in the context of immunity (e.g., macrophages) but barely in the context of nutrition.[34] We therefore investigated the spatial gene expression profiles of endocytic pathway markers and transcription factors in the nutritive phagocytic cells of the *Nematostella* mesenteries (Figures 2 and S2). Genes were selected for analysis based on either their informative value as conserved marker genes for cellular processes (e.g., phagocytosis, lysosomal digestion), their co-occurrence in putative endocytic "metacells" of a whole-polyp, single-cell RNA sequencing dataset[35] (Table S1; Data S1), or as a spatial reference to juvenile nutrient storage regions.[36] We found that *lipopolysaccharide binding protein/bactericidal permeability-increasing protein* (*lbp/bpi*; Figure S2A) and C-type lectin *mannose receptor* (*mannR*; Figure S2B) gene orthologs of *Nematostella* are specifically expressed in the endocytic TT (both genes), IT (*lbp/bpi* only), and SGE (*mannR* only) (Figures 2A–2B″ and 2J). Their bilaterian orthologs recognize bacterial lipopolysaccharide and glycans as well as soluble macromolecules and large particulate matter. MannR is additionally known to induce phagocytosis and clathrin-mediated endocytosis.[37–39] Their expression in *Nematostella* thus supports a dual role for endocytic regions in both immunity and nutrition. Next, we checked the expression of *Nematostella* orthologs of *cdc42* and *rhoA* genes, which play key roles in phagocytic cup formation, and of *low-density lipoprotein receptor-like* (*ldlr-like*), *clathrin light chain* (*clatLC*), and *clathrin heavy chain* (*clatHC*) genes, all encoding for proteins involved in clathrin-mediated endocytosis. Expression of all these genes overlaps with bead uptake in IT, TT, and SGE regions (Figures 2C–2G″ and 2J), supporting phagocytosis and clathrin-mediated endocytosis as their main endocytic mechanisms. Additionally, the predominant expression of gene orthologs encoding for glycosidases (*α-glucosidase*, *α-mannosidase*), proteases (*cathepsin*), and cholesterol transport/recycling (*npc2*) proteins, in all or a subset of the three endocytic mesenterial regions (Figures S2C–S2K), supports increased intracellular digestion levels. In juvenile *Nematostella*, the median, lipid-storing part of the mesentery was previously reported to co-express a combination of *foxC, six4/5*, and *nkx3/bagpipe* transcription factor genes, revealing striking similarities to lateral mesoderm derivatives of bilaterians, such as somatic gonad or nutrient storage tissues (e.g., insect fat body).[36,40] How this juvenile region relates to adult endocytic structures was yet to be determined. While nkx3/*bagpipe* expression levels were below detection limits, *foxC* and *six4/5* genes were expressed in all endocytic regions of the adult mesentery (Figures 2H–2J), indicating similarities to the lipid-uptaking region of juvenile mesenteries.

In order to test how the expression profile of *Nematostella* endocytic cells compares with putative trophic phagocytes or lipid-storing cells of other animals, we searched previously published single-cell transcriptomes of the stony coral *Stylophora pistillata*, the planarian *Schmidtea mediterranea*, and the sponge *Amphimedon queenslandica* for metacells/clusters that share at least 2 of our candidate genes (Table S1; Data S1). We found the highest overlap with metacells/clusters identified as *Stylophora* gastrodermis or "alga-hosting" cells, *Schmidtea cathepsin+* parenchymal, intestinal, or neuronal cells, or as *Amphimedon* pinacocytes or archeocytes. Notably, all identified metacells/clusters (except *Schmidtea* neural cells) refer to cell types

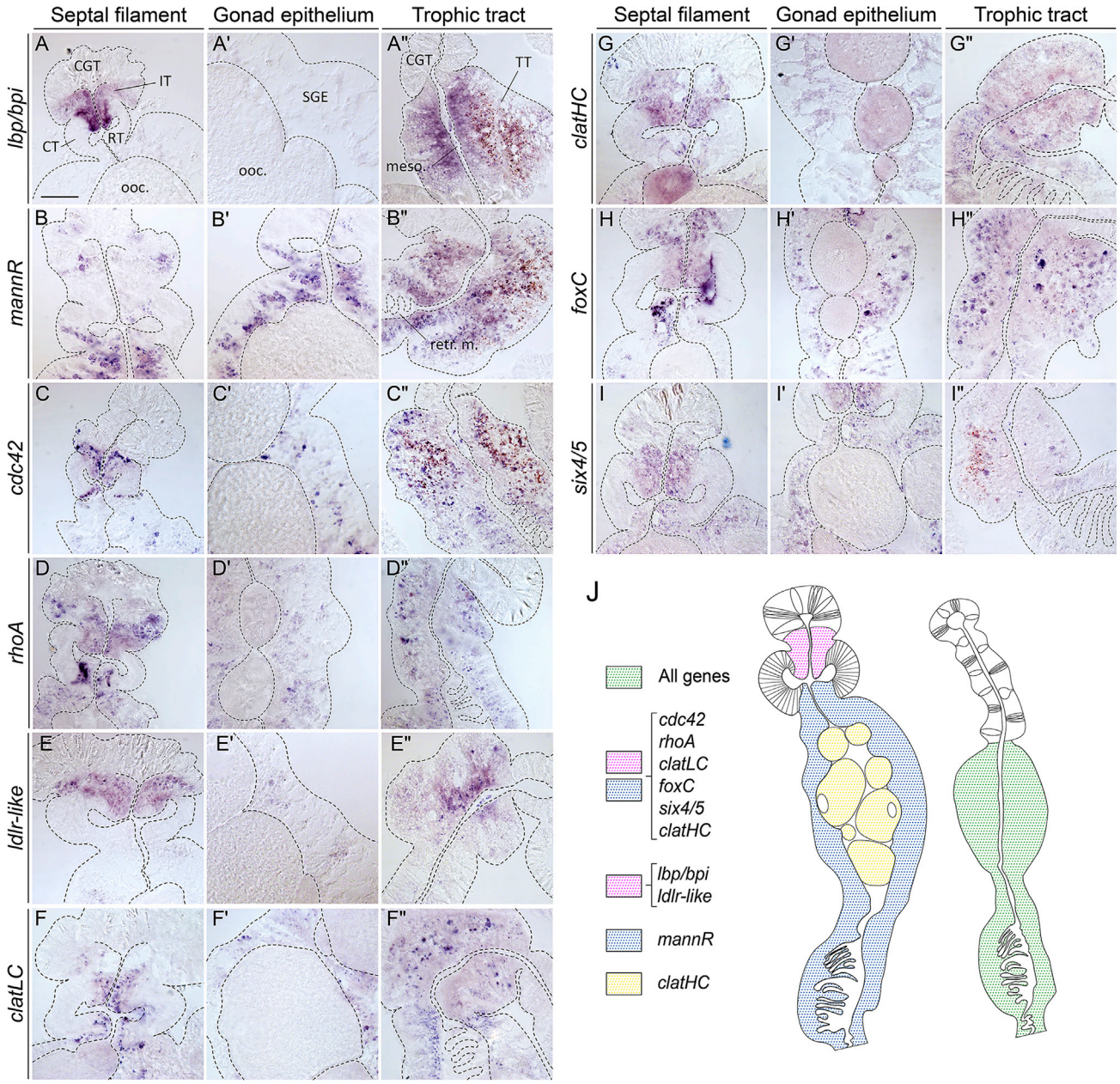

Figure 2. Phagocytosis- and receptor-mediated endocytosis-related genes are expressed in endocytic regions of the mesenteries

(A–I″) mRNA expression patterns of *Nematostella* orthologs of the *lbp/bpi* (A–A″), *mannR* (B–B″), *cdc42* (C–C″), *rhoA* (D–D″), *ldlr-like* (E–E″), *clatLC* (F–F″), *clatHC* (G–G″), *foxC* (H–H″), and *six4/5* (I–I″) genes in the septal filament (A–I), gonad epithelium (A′–I′), and trophic tract (A″–I″). See text for gene descriptions.

(J) Summary schematics of gene expression patterns. Distal end of mesenteries oriented to the top.

All data figures represent cross-sections of adult *Nematostella* mesenteries stained by colorimetric *in situ* hybridization. Scale bar, 50 μm. CT, ciliated tract; CGT, cnidoglandular tract; *clatHC* and *LC*, clathrin heavy and light chain; SGE, somatic gonad epithelium; IT, intermediate tract; *lbp/bpi*, lipopolysaccharide binding protein/bactericidal permeability increasing protein; *ldlr-like*, low-density lipoprotein receptor-like gene; *mannR,* mannose receptor; meso, mesoglea; ooc, oocyte; RT, reticulate tract; retr. m, retractor muscle; TT, trophic tract.

See also Figure S2.

previously characterized as phagocytosic and/or lipid-storing. In addition, the presence of *six4/5* or *foxC* orthologs in a subset of identified metacells/clusters throughout all datasets supports a potential conservation of *six4/5* and *foxC* in endocytic and/or lipid-storing cell types across animals.

Our characterization of cellular particle uptake modalities and gene expression profiles has revealed that distinct mesenterial regions are specialized in food particle endocytosis. We next tested whether these regions provide dietary nutrients to the oocytes by studying the cells and molecules

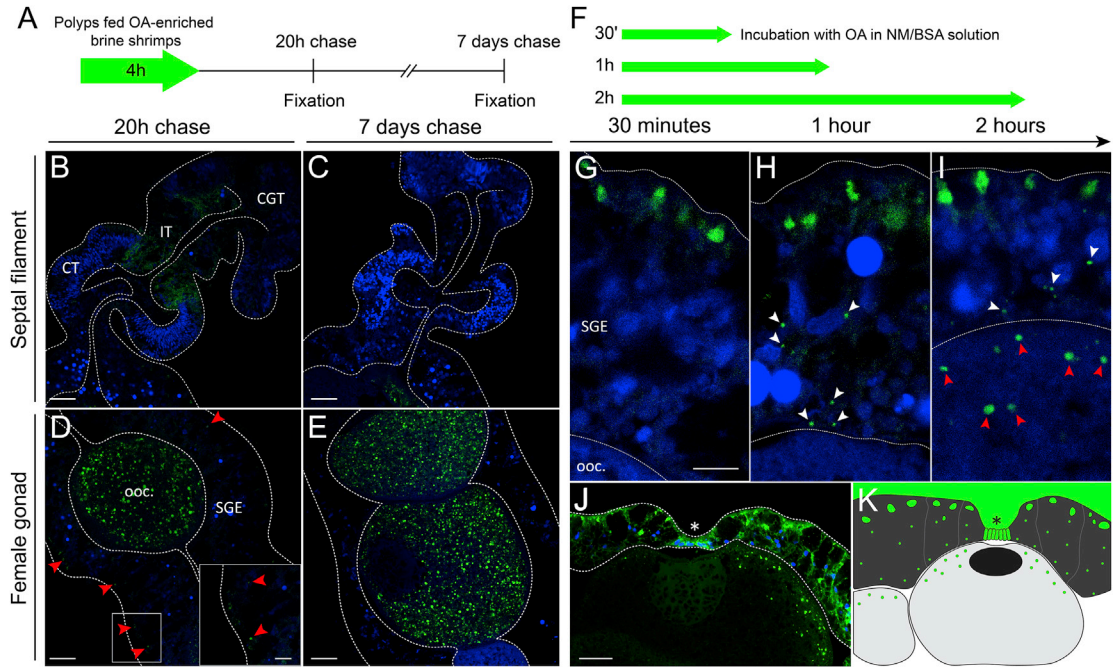

Figure 3. *Trans*-epithelial transport of alkyne-OA occurs from the gastric cavity into oocytes

(A–E) A pulse-chase experiment using a 4-h pulse of alkyne-OA-enriched brine shrimps reveals long-term changes in lipid mobilization. In the IT, alkyne-oleic acid (green) is detected faintly after 20 h (B), but not after 7 days (C) of chase. Similarly, small positive vesicles are present in the gonad epithelium after 20 h (D and insert within, red arrowheads) but are absent after 7 days of chase (E). Note that alkyne-OA is present in oocytes after both 20 h and 7 days of chase (D and E). (F–K) Incubation with BSA-coupled alkyne-OA over short time periods reveals the timeline and dynamics of alkyne-OA uptake. Alkyne-OA is progressively detected near the apical surface of SGE cells after 30 min (G), their basal half after 1 h (H, white arrowheads), and in oocytes after 2 h of incubation (I, red arrowheads). Signal is also present in cells of the trophonema (J, asterisk). (K) Schematic summary of *trans*-epithelial alkyne-OA transport.

Distal end of mesenteries oriented to the top (B–E) or left (G–K). All data figures show single confocal plane images of adult female *Nematostella* mesentery cross-sections. Blue, DAPI nuclear stain. Scale bars, 25 μm (B–E), 10 μm (D and G–J, insert), and 25 μm (J). CGT, cnidoglandular tract; CT, ciliated tract; IT, intermediate tract; OA, oleic acid; ooc, oocyte, SGE, somatic gonad epithelium.

See also Figure S3.

mediating the transport of fatty acids from the gastric cavity into the oocytes.

Dietary fatty acids reach the oocyte by *trans*-epithelial transport

Spatial detection of neutral lipid storage using Oil Red O (ORO) staining confirmed that lipids are a major yolk component in *Nematostella* (Figure S3A). It also showed high levels of neutral lipids largely overlapping with endocytic regions (SGE, IT, and TT) in both male and female adults (Figures S3A–S3C). In contrast, lipid levels appeared low in non-endocytic regions such as the ciliated tract (CT) or cnidoglandular tract (CGT), suggesting that only specialized endocytic cells and gametes possess lipid transport or storage abilities. We explored the dynamics of fatty acid uptake and transport from the gastric cavity toward the oocyte by developing a whole-body pulse-chase assay using a "clickable," alkyne-modified oleic acid[41] (alkyne-OA). Previous studies used alkyne-OA to reliably mimic oleic acid and study its metabolism in yeast, *Drosophila*, and mammalian cells.[41] As oleic acid is abundantly found in anthozoan storage lipids, it is well-suited to track dietary fatty acids in *Nematostella*.[42,43] A 4-h-pulse/20-h-chase experiment using alkyne-OA-enriched brine shrimps resulted in labelling of the IT, the SGE (Figures 3A, 3B, and 3D), and the distal TT (Figures S3D–S3H), largely overlapping with endocytic regions. Notably, both IT and SGE became devoid of alkyne-OA after 7 days of chase (Figures 3C and 3E), suggesting lipid catabolism or translocation. In contrast, alkyne-OA in cells of the TT shifted location from the apical side of distal cells (at 20-h chase; Figures S3E and S3G) to the basal side of proximal cells (at 7-day chase; Figures S3F and S3H), with small vesicles apparent in the mesoglea, possibly hinting at basolateral lipid secretion into the ECM (Figure S3H, arrowheads).

In oocytes, alkyne-OA strongly accumulated in vesicles after 20 h and 7 days of chase (Figures 3D and 3E), confirming major dietary fatty acid movement from the gastric cavity into ECM-based oocytes. We increased the temporal control and resolution of alkyne-OA delivery by directly injecting alkyne-OA/BSA solution into the gastric cavity (Figures 3F–3K and S3I–S3N). This optimized delivery method yielded similar results to feeding enriched brine shrimps, which relied on individual rates of extracellular digestion (compare Figures S3J and S3K with Figures 3B–3E; Figures S3L and S3M with Figures S3E and S3F). We found that 30 min after delivery, alkyne-OA localized to large apical vesicles in SGE cells (Figure 3G). Within 1 h of incubation, smaller vesicles appeared in median and basal regions of SGE cells, suggesting rapid intracellular apical-to-basal translocation of alkyne-OA (Figure 3H, white arrowheads). Between 1 and 2 h after delivery, alkyne-OA vesicles started accumulating intracellularly at the

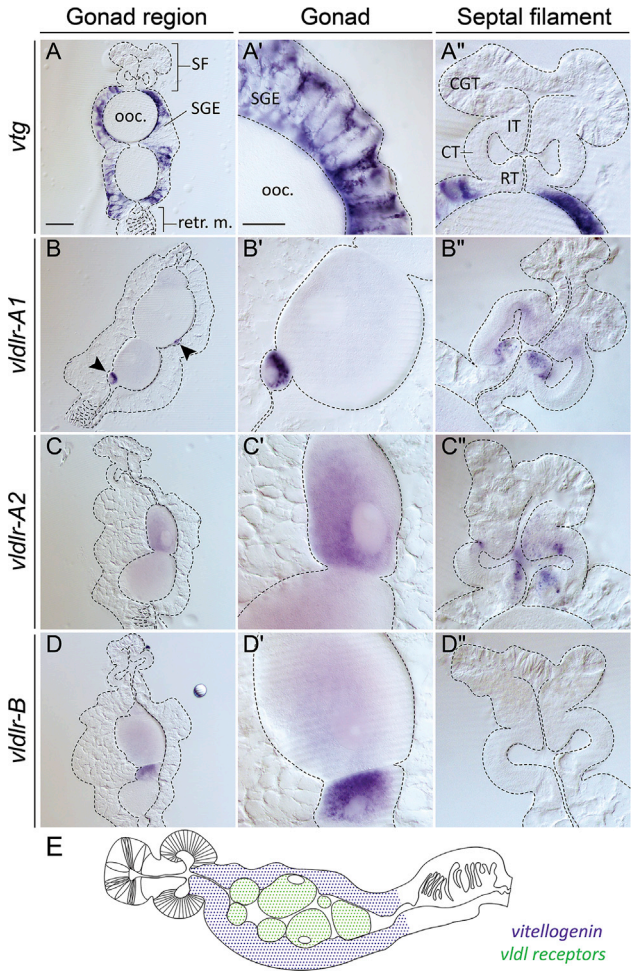

Figure 4. Complementary expression of *Nematostella vtg* and *vldlr* gene orthologs supports lipid transport from the SGE into oocytes

(A–D″) mRNA expression patterns of *vtg* (A–A″) and its potentially conserved lipoprotein receptors *vldlr-A1* (B–B″, small eggs marked by arrowheads), *vldlr-A2* (C–C″), and *vldlr-B* (D–D″) in somatic gonad epithelium and oocytes, respectively. *vldlr-A1* and *-A2* are additionally expressed in cells of the septal filament (B″ and C″).

(E) Schematic summary of the complementarity of *vtg/vldlr* expression patterns. Note that for reasons of clarity and due to the uncertainty of potential overlap between *vldlr-A1* and *-A2* expression in septal filament cells, their expression was omitted from the schematic.

Distal end of mesenteries oriented to the top (A–D″) or left (E). All data figures show cross-sections of adult female *Nematostella* mesenteries (gonad region). Scale bars, 100 μm (A–D) and 50 μm (A′–D″). CT, ciliated tract; CGT, cnidoglandular tract; SGE, somatic gonad epithelium; IT, intermediate tract; ooc, oocyte; RT, reticulate tract; *vldlr*, very low-density lipoprotein receptor; *vtg*, vitellogenin.

See also Figure S4.

periphery of the oocyte adjacent to the SGE (Figures 3I and 3K, red arrowheads; Figure S3N). A 24-h-long incubation revealed the uptake of alkyne-OA in trophonema cells of the female SGE (24 out of 24 trophonemata; Figures 3J and 3K). These observations are in full agreement with the trans-epithelial transport of alkyne-OA from the gastric cavity through the SGE into oocytes via the surrounding ECM. Our inability to detect alkyne-OA in the ECM could indicate a rapid clearance by high levels of endocytosis into oocytes, which is strongly supported by ultrastructural observations.[25] Notably, the absence of endocytic activity in trophonema cells and of alkyne-OA in the adjacent oocyte region questions their previously proposed role as main nutrient-shuttling cells in *Nematostella* and other sea anemones.[22,24,44] We were next interested to investigate how lipid transport through the SGE and ECM could be mediated on the molecular level.

To do so, we studied the expression of the single *Nematostella* orthologs of *vtg* and *apoB* apolipoprotein genes (Figure S4A) and three *Nematostella vldl receptor* (*vldlr*) paralogs conserved among sea anemones and corals (Figures S4B and S4C). We confirm previous reports from *Nematostella* and other anthozoans that the SGE expresses high levels of *vtg* transcripts (Figures 4A–4A″).[45–48] In contrast, no *vtg* transcript was detected in oocytes despite Vtg representing ±60% of the protein content of the mature egg in *Nematostella*.[49] As cytoplasmic connections between oocytes and the gonad epithelium are absent,[25,50] this indicates that Vtg protein accumulation in anthozoan oocytes is largely dependent on endocytosis. *vldlr-A1*, *-A2*, and *-B* genes (Figures S4B and S4C) are all expressed in growing oocytes of different sizes (Figures 4B–4E), supporting a role in receptor-mediated apolipoprotein uptake during vitellogenesis. *vldlr-A1* and *vldlr-A2* are additionally expressed in uncharacterized cells of the IT and reticulate tract of the septal filament (SF) (Figures 4B″ and 4C″). Altogether, our data strongly suggest that Vtg mediates lipid transport from SGE cells into growing oocytes by VLDLR-mediated endocytosis, as widely found among bilaterians.[4,51]

Although ApoB-encoding genes are found in genomes of bilaterians, cnidarians, and placozoans (Figure S4A), their expression profiles and role in lipid transport have not been characterized in any non-bilaterian animal. In *Nematostella*, *apoB* expression colocalizes with *vtg* expression in the SGE but further extends to the IT and TT, thus fully overlapping with endocytic regions (Figures 5A–5C). This broader expression suggests a role for ApoB in lipid transport beyond vitellogenesis, as typically found in bilaterians.[52] To further explore this possibility, we aimed to study the localization of ApoB proteins and their potential colocalization with alkyne-OA. We therefore generated a transgenic reporter line using CRISPR-Cas9-mediated knockin technology, resulting in a genomically encoded, C-terminal ApoB-PSmOrange fusion protein (Figure S5). As expected, ApoB-PSmOrange protein detected by immunofluorescence localizes to endocytic regions with high *apoB* transcript levels (compare Figures 5A–5C with 5D–5I). Large ApoB-PSmOrange-containing vesicles are distributed throughout the cells of the IT (Figures 5D and 5E) and male SGE (Figure 5H). In cells of the TT and female SGE, similarly sized vesicles accumulate apically (Figures 5F, 5G, and 5I). Growing oocytes were devoid of the ApoB-PSmOrange signal (Figure 5G), as supported by low levels of ApoB protein detected by mass spectrometry in spawned eggs.[49] Notably, however, ApoB-PSmOrange protein was detected in spermaries, with higher intensities in peripheral, immature cells compared with central, mature spermatozoa (Figure 5H). Here, ApoB-PSmOrange and alkyne-OA localize to adjacent but clearly distinct vesicles (Figures 6E–6E″). While we found broad overlap between tissues with high ApoB-PSmOrange protein and alkyne-OA uptake levels, we detected only partial intracellular colocalization in the male and female SGE after a 2-h alkyne-OA pulse (Figures 6A–6B″).

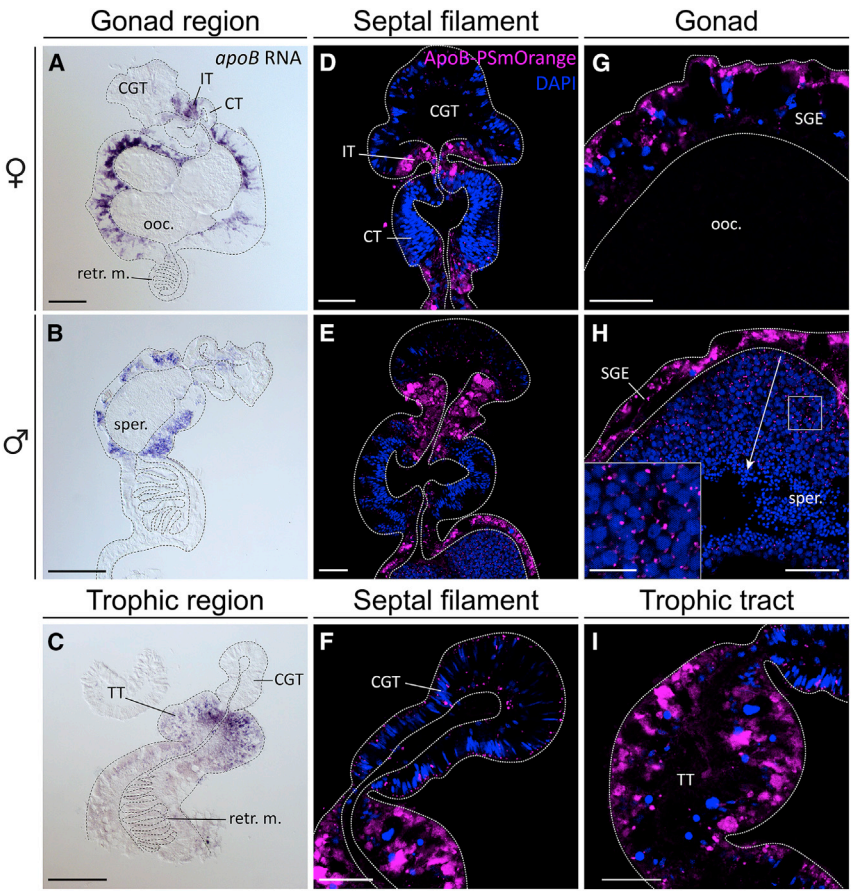

Figure 5. *Nematostella apoB* mRNA and ApoB-PSmOrange fusion protein localization suggests a role for ApoB in spermatogenesis but not in vitellogenesis

(A–C) *apoB* mRNA expression in the gonad region of female (A) and male (B) polyps, and in the trophic region (C).

(D–I) ApoB-PSmOrange protein localization (magenta) is consistent with *apoB in situ* hybridization data (A–C) in the TT, IT, and SGE of female and male gonad regions. Notably, ApoB-PSmOrange is found in spermaries (H). Insert in (H) shows close-up of the boxed region. A peripheral to central gradient of decreasing signal intensity coincides with the progression of sperm cells maturation stages (arrow).

Distal end of mesenteries oriented to the top (A–F and I) or left (G and H). Cross-sections of adult *Nematostella* mesenteries. Blue, DAPI nuclear stain. All fluorescent images represent single confocal planes. Scale bars, 100 μm (A–C), 25 μm (D–I), and 10 μm closed-up (H). CT, ciliated tract; CGT, cnidoglandular tract; SGE, somatic gonad epithelium; IT, intermediate tract; ooc, oocyte; retr. m, retractor muscle; sper, spermary; TT, trophic tract.

See also Figures S4 and S5.

Interested to investigate a potential role for ApoB in systemic lipid transport, we compared the distribution of ApoB-PSmOrange and alkyne-OA between a 2-h pulse (Figures 6A–6B″) and a 4-h pulse, followed by a 7-day chase (Figures 6C–6E″). Strikingly, we found ApoB-PSmOrange/alkyne-OA colocalization in mesenchymal-like mesogleal cells of the trophic region only in the pulse-chase experiment (Figures 6C–6D″). This result shows that oleic acid became mobilized in endocytic epithelial cells, as indicated before by intracellular apical-to-basal movements within TT cells (Figures S3E–S3H), and translocated through the ECM into mesogleal cells. The most likely explanation, to be tested in future studies, is that ApoB-mediated lipid transport from epithelial to mesogleal cells enables subsequent systemic lipid distribution in sea anemones.

DISCUSSION

In many bilaterian animals, dietary nutrients travel from the gut epithelium to oocytes via ECM-based circulatory systems or, more rarely, through coelomic cavity fluids.[4,53,54] Due to the lack of data from non-bilaterian animals, the emergence of systemic nutrient transport and its underlying cellular and molecular features during animal evolution has remained speculative.[1–3] We have, therefore, retraced the cellular path of dietary nutrients, more specifically lipids, from the gastric cavity to the oocytes during vitellogenesis in the sea anemone *Nematostella vectensis*. We have shown that although the entire gastrodermal epithelium is in direct contact with food particles and nutrients, it does not show a uniform distribution of phagocytosis, micropinocytosis, and lysosomal activities. Instead, our analyses of bead uptake assays and marker gene expression show that these activities are enriched in the tentacle gastrodermis as well as the IT, SGE, and TT mesenterial regions. In corals and symbiotic sea anemones (e.g., *Exaiptasia*), carbon-fixing *Symbiodinium sp.* dinoflagellates locate mainly to the tentacle gastrodermis and the IT and SGE regions.[23,55] These parallels confirm the importance of these regions in nutrient acquisition in sea anemones and corals and raise questions about the symbionts' ability to permanently populate these highly endocytic regions in some anthozoan species but not in others.

As our molecular knowledge of animal phagocytosis relies almost entirely on the study of innate immunity cell types (e.g., macrophages), we provide one of the first molecular characterizations of animal trophic phagocytes.[34] Notably, the set of genes found expressed in nutritive endocytic regions in *Nematostella*, composed of immunity-related pattern recognition proteins (LPS/BPI, C-type lectins), phagocytic cup and clathrin-mediated endocytosis components, as well as lysosomal enzymes and transporters, is largely shared with immune cells in vertebrates and flies.[56–59] This raises the question of whether *Nematostella* trophic phagocytes are bi-functional and carry out nutritive as well as immunity-related functions, e.g., in controlling the gastrodermal surface microbiome composition or preventing symbiont settlement. Currently, a reconstruction of trophic and immune phagocytic cell-type evolution remains difficult, as only little comparative molecular data are available from bilaterian trophic phagocytes.[34,60] Nevertheless, our comparison with available single-cell transcriptomes reveals expression profile

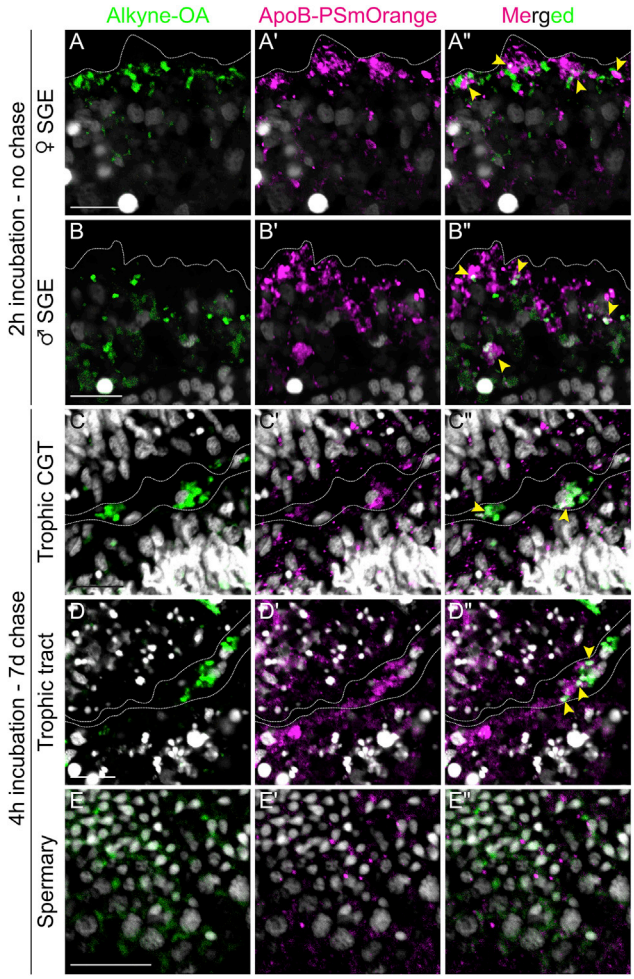

Figure 6. Colocalization of alkyne-oleic acid and ApoB-PSmOrange in a subset of SGE vesicles and in mesogleal cells of the trophic region

(A–E) Codetection of alkyne-OA (green) and ApoB-PSmOrange (magenta) after a 2 h alkyne-OA pulse (A–B″) or after a 4 h pulse and 7 days of chase (C–E″).

(A and B) Some intracellular vesicles (A″ and B″, arrowheads) show colocalization of alkyne-OA with ApoB-PSmOrange in the female (A–A″) or male SGE (B–B″).

(C and D) Interestingly, mesogleal cells with alkyne-OA and ApoB-PSmOrange colocalization are found in the trophic cnidoglandular tract (C–C″, arrowheads) and trophic tract (D–D″, arrowheads). Note the presence of nuclei adjacent to signal colocalization.

(E) In spermaries, alkyne-OA and ApoB-PSmOrange vesicles locate adjacently but do not overlap (E–E″). Distal end of mesenteries oriented to the left.

Dotted lines in (C)–(D″) delimit the mesoglea. All images represent single confocal plane images of adult *Nematostella* mesenteries cross-sections. Gray, Hoechst 33342 nuclear stain. Scale bars, 10 μm. CGT, cnidoglandular tract; SGE, somatic gonad epithelium.

similarities, mainly with trophic phagocytic cells such as coral alga-hosting and gastrodermal cells, planarian phagocytic parenchymal and intestinal cells,[34,61] and sponge pinacocytes and archeocytes.[40] The shared expression of *foxC and six4/5* transcription factors in endocytic/lipid-storing cells of *Nematostella*, corals, planarians, and sponges is reminiscent of their co-expression in lateral mesoderm regions of bilaterians, whose typical derivatives include blood immune cells, nutrient storage tissues (e.g., insect fat body), or somatic gonad tissue.[62] More in-depth analysis of a broader set of species is needed to reveal the evolutionary relationship of endocytic/lipid-storing cell types across animal phyla.

We identified the SGE as highly relevant among mesenterial endocytic regions for dietary nutrient transport during vitellogenesis. Indeed, our data show that the SGE plays an important role in dietary particle and lipid uptake and as a Vtg-producing tissue. Our alkyne-oleic acid tracking experiments strongly suggest that dietary fatty acids are rapidly absorbed and transported through the SGE into the ECM before being internalized via endocytosis by oocytes, as corroborated by ultrastructural observations.[25] As Vtg transcripts are highly expressed in the SGE and the corresponding protein is highly abundant in the mature egg,[49] we propose that it constitutes the key lipid transporter from the SGE through the ECM into oocytes during vitellogenesis in *Nematostella*. We found three *Nematostella vldl receptor* paralogs expressed during oocyte growth, of which VLDLR-B was previously identified in the proteome of mature eggs.[49] These results support the idea that Vtg endocytosis is mediated by VLDL receptors in *Nematostella*. Together, our data suggest that a Vtg ligand/VLDL receptor pair has been evolutionarily conserved during vitellogenic lipid transport since the last common bilaterian-cnidarian ancestor.

ApoB protein, involved in systemic lipid transport in bilaterians, appears to have no direct role during vitellogenesis in *Nematostella*. Although abundantly found in the SGE, it was detected at low levels in oocytes via mass spectrometry[49] and below immunofluorescence detection limits. Instead, we found ApoB-positive vesicles in spermatogonia or immature spermatozoa, suggesting a role in lipid transport or metabolism during spermatogenesis. Loss of ApoB function has been linked to male infertility so far only in mice[63,64] and further investigations are necessary to corroborate an evolutionarily conserved function of ApoB during animal spermatogenesis. In addition to the SGE, ApoB-PSmOrange protein levels were high in all other endocytic tissues of *Nematostella*. Partial colocalization with apical alkyne-OA suggests that ApoB might function in intracellular fatty acid transport. Strikingly, we also found ApoB protein broadly colocalizing with pulse-chased alkyne-OA in single mesogleal cells. Based on location and lipid content, these cells are highly reminiscent of motile amoebocytes that were previously identified in several anthozoans.[65–67] Our observation therefore supports previous assumptions that amoebocytes function in systemic nutrient transport via the mesoglea in anthozoans.[65–67]

A prevalent hypothesis has stated that bilaterian circulatory systems evolved from a simple ECM-based fluid and nutrient transport system[2] but has so far lacked experimental support. Here, we show first evidence that Vtg/ApoB- and VLDLR-mediated lipid transport through the ECM space is not only conserved in bilaterians but also found in a sea anemone. We suggest, therefore, that the local, ECM-based transport of yolk precursors predates the cnidarian-bilaterian split. Furthermore, we propose that this simple nutrient transport system formed a framework for the evolution of intricate ECM-based circulatory systems, ensuring a systemic nutrient supply in increasingly large and complex bilaterians.

STAR★METHODS

Detailed methods are provided in the online version of this paper and include the following:

- KEY RESOURCES TABLE
- RESOURCE AVAILABILITY
  - Lead contact
  - Materials availability
  - Data and code availability
- EXPERIMENTAL MODEL AND SUBJECT DETAILS
  - *Nematostella vectensis* culture
- METHOD DETAILS
  - Particle uptake assays and tissue fixation
  - Candidate gene identification and orthology, single-cell datasets comparison
  - Phylogeny
  - Gene cloning and RNA probe synthesis
  - *In situ* hybridization
  - Alkyne-oleic acid assays and Click-it reaction
  - CRISPR-Cas9 mediated generation of ApoB-PSmOrange knock-in line
  - Immunofluorescence
  - Cryotome sectioning
  - Oil Red O staining
  - Transmitted light and confocal imaging

SUPPLEMENTAL INFORMATION

Supplemental information can be found online at https://doi.org/10.1016/j.cub.2022.08.039.

ACKNOWLEDGMENTS

We thank E. Hambleton for kindly providing plasmids encoding *npc2* genes, Eilen Myrvold and Lavina Jubek for taking excellent care of the Sars Centre *Nematostella* culture, and all Steinmetz lab members for helpful discussions and feedback on the manuscript. This work was supported by the Sars Centre core budget.

AUTHOR CONTRIBUTIONS

M.L. and P.R.H.S. conceived, designed, and performed experiments; analyzed data; and wrote the manuscript. P.M.-P. performed experiments and analyzed data.

DECLARATION OF INTERESTS

The authors declare no competing interests.

Received: March 7, 2022
Revised: July 25, 2022
Accepted: August 15, 2022
Published: September 8, 2022

REFERENCES

1. Schmidt-Rhaesa, A. (2007). The Evolution of Organ Systems (Oxford University Press).
2. Ruppert, E.E., and Carle, K.J. (1983). Morphology of metazoan circulatory systems. Zoomorphology *103*, 193–208.
3. Hartenstein, V., and Mandal, L. (2006). The blood/vascular system in a phylogenetic perspective. BioEssays *28*, 1203–1210.
4. Eckelbarger, K.J., and Hodgson, A.N. (2021). Invertebrate oogenesis–a review and synthesis: comparative ovarian morphology, accessory cell function and the origins of yolk precursors. Invertebr. Reprod. Dev. *65*, 71–140.
5. Babin, P.J., Bogerd, J., Kooiman, F.P., Van Marrewijk, W.J.A., and Van der Horst, D.J. (1999). Apolipophorin II/I, apolipoprotein B, vitellogenin, and microsomal triglyceride transfer protein genes are derived from a common ancestor. J. Mol. Evol. *49*, 150–160.
6. Smolenaars, M.M.W., Madsen, O., Rodenburg, K.W., and Van Der Horst, D.J. (2007). Molecular diversity and evolution of the large lipid transfer protein superfamily. J. Lipid Res. *48*, 489–502.
7. Wahli, W., Dawid, I.B., Ryffel, G.U., and Weber, R. (1981). Vitellogenesis and the vitellogenin gene family. Science *212*, 298–304.
8. Wallace, R.A. (1985). Vitellogenesis and oocyte growth in nonmammalian vertebrates. Dev. Biol. *1*, 127–177.
9. Polzonetti-Magni, A.M., Mosconi, G., Soverchia, L., Kikuyama, S., and Carnevali, O. (2004). Multihormonal control of vitellogenesis in lower vertebrates. Int. Rev. Cytol. *239*, 1–46.
10. Palm, W., Sampaio, J.L., Brankatschk, M., Carvalho, M., Mahmoud, A., Shevchenko, A., and Eaton, S. (2012). Lipoproteins in *Drosophila melanogaster*—assembly, function, and influence on tissue lipid composition. PLoS Genet. *8*, e1002828.
11. Kawooya, J.K., and Law, J.H. (1988). Role of lipophorin in lipid transport to the insect egg. J. Biol. Chem. *263*, 8748–8753.
12. Van der Horst, D.J., Roosendaal, S.D., and Rodenburg, K.W. (2009). Circulatory lipid transport: lipoprotein assembly and function from an evolutionary perspective. Mol. Cell. Biochem. *326*, 105–119.
13. Dieckmann, M., Dietrich, M.F., and Herz, J. (2010). Lipoprotein receptors-an evolutionarily ancient multifunctional receptor family. Biol. Chem. *391*, 1341–1363.
14. Strickland, D.K., Gonias, S.L., and Argraves, W.S. (2002). Diverse roles for the LDL receptor family. Trends Endocrinol. Metab. *13*, 66–74.
15. Tufail, M., and Takeda, M. (2009). Insect vitellogenin/lipophorin receptors: molecular structures, role in oogenesis, and regulatory mechanisms. J. Insect Physiol. *55*, 87–103.
16. Hayward, A., Takahashi, T., Bendena, W.G., Tobe, S.S., and Hui, J.H.L.L. (2010). Comparative genomic and phylogenetic analysis of vitellogenin and other large lipid transfer proteins in metazoans. FEBS Lett. *584*, 1273–1278.
17. Riesgo, A., Farrar, N., Windsor, P.J., Giribet, G., and Leys, S.P. (2014). The analysis of eight transcriptomes from all Poriferan classes reveals surprising genetic complexity in sponges. Mol. Biol. Evol. *31*, 1102–1120.
18. Wu, L.T., Hui, J.H.L., and Chu, K.H. (2013). Origin and evolution of yolk proteins: expansion and functional diversification of large lipid transfer protein superfamily. Biol. Reprod. *88*, 102.
19. Brusca, R.C., Moore, W., and Shuster, S.M. (2016). Invertebrates, Third Edition (Sinauer Associates).
20. Park, T.Y., Woo, J., Lee, D.J., Lee, D.C., Lee, S.B., Han, Z., Chough, S.K., and Choi, D.K. (2011). A stem-group cnidarian described from the mid-Cambrian of China and its significance for cnidarian evolution. Nat. Commun. *2*, 442.
21. Ou, Q., Han, J., Zhang, Z., Shu, D., Sun, G., and Mayer, G. (2017). Three Cambrian fossils assembled into an extinct body plan of cnidarian affinity. Proc. Natl. Acad. Sci. USA *114*, 8835–8840.
22. Shick, J.M. (1991). A Functional Biology of Sea Anemones, P. Calow, ed. (Springer Netherlands).
23. Van-Praët, M. (1985). Nutrition of sea anemones. Adv. Mar. Biol. *22*, 65–99.
24. Fautin, D.G., and Mariscal, R.M. (1991). Cnidaria: Anthozoa. In Microscopic Anatomy of Invertebrates: Placozoa, Porifera, Cnidaria and Ctenophora, *2*, F. Harrison, and J. Westfall, eds. (Wiley-Liss), pp. 267–358.

25. Eckelbarger, K.J., Hand, C., and Uhlinger, K.R. (2008). Ultrastructural features of the trophonema and oogenesis in the starlet sea anemone, *Nematostella vectensis* (Edwardsiidae). Invertebr. Biol. *127*, 381–395.

26. Fautin, D.G. (2002). Reproduction of Cnidaria. Can. J. Zool. *80*, 1735–1754.

27. Snyder, G.A., Eliachar, S., Connelly, M.T., Talice, S., Hadad, U., Gershoni-Yahalom, O., Browne, W.E., Palmer, C.V., Rosental, B., and Traylor-Knowles, N. (2021). Functional characterization of Hexacorallia phagocytic cells. Front. Immunol. *12*, 662803.

28. Okubo, N., Tamura-Nakano, M., and Watanabe, T. (2020). Experimental observation of microplastics invading the endoderm of anthozoan polyps. Mar. Environ. Res. *162*, 105125.

29. Van-Praët, M. (1980). Absorption des substances dissoutes dans le milieu, des particules et des produits de la digestion extracellulaire chez *Actinia equina* (Cnidaria, Actiniaria). Reprod. Nutr. Dev. *20*, 1393–1399.

30. Underhill, D.M., and Goodridge, H.S. (2012). Information processing during phagocytosis. Nat. Rev. Immunol. *12*, 492–502.

31. Gray, M., and Botelho, R.J. (2017). Phagocytosis: hungry, hungry cells. Methods Mol. Biol. *1519*, 1–16.

32. Lancaster, C.E., Ho, C.Y., Hipolito, V.E.B., Botelho, R.J., and Terebiznik, M.R. (2019). Phagocytosis: what's on the menu? Biochem. Cell Biol. *97*, 21–29.

33. Moiseeva, E., Rabinowitz, C., Paz, G., and Rinkevich, B. (2017). Histological study on maturation, fertilization and the state of gonadal region following spawning in the model sea anemone, *Nematostella vectensis*. PLoS One *12*, 1–17.

34. Hartenstein, V., and Martinez, P. (2019). Phagocytosis in cellular defense and nutrition: a food-centered approach to the evolution of macrophages. Cell Tissue Res. *377*, 527–547.

35. Sebé-Pedrós, A., Saudemont, B., Chomsky, E., Plessier, F., Mailhé, M.P., Renno, J., Loe-Mie, Y., Lifshitz, A., Mukamel, Z., Schmutz, S., et al. (2018). Cnidarian cell type diversity and regulation revealed by whole-organism single-cell RNA-seq. Cell *173*, 1520–1534.e20.

36. Steinmetz, P.R.H., Aman, A., Kraus, J.E.M., and Technau, U. (2017). Gut-like ectodermal tissue in a sea anemone challenges germ layer homology. Nat. Ecol. Evol. *1*, 1535–1542.

37. Rosales, C., and Uribe-Querol, E. (2017). Phagocytosis: a fundamental process in immunity. BioMed Res. Int. *2017*, 9042851.

38. Baron, O.L., Deleury, E., Reichhart, J.M., and Coustau, C. (2016). The LBP/BPI multigenic family in invertebrates: evolutionary history and evidences of specialization in mollusks. Dev. Comp. Immunol. *57*, 20–30.

39. East, L., and Isacke, C.M. (2002). The mannose receptor family. Biochim. Biophys. Acta *1572*, 364–386.

40. Steinmetz, P.R.H. (2019). A non-bilaterian perspective on the development and evolution of animal digestive systems. Cell Tissue Res. *377*, 321–339.

41. Thiele, C., Papan, C., Hoelper, D., Kusserow, K., Gaebler, A., Schoene, M., Piotrowitz, K., Lohmann, D., Spandl, J., Stevanovic, A., et al. (2012). Tracing fatty acid metabolism by click chemistry. ACS Chem. Biol. *7*, 2004–2011.

42. Revel, J., Massi, L., Mehiri, M., Boutoute, M., Mayzaud, P., Capron, L., and Sabourault, C. (2016). Differential distribution of lipids in epidermis, gastrodermis and hosted *Symbiodinium* in the sea anemone *Anemonia viridis*. Comp. Biochem. Physiol. A Mol. Integr. Physiol. *191*, 140–151.

43. Papina, M., Meziane, T., and van Woesik, R. (2003). Symbiotic zooxanthellae provide the host-coral *Montipora digitata* with polyunsaturated fatty acids. Comp. Biochem. Physiol. B Biochem. Mol. Biol. *135*, 533–537.

44. Larkman, A.U., and Carter, M.A. (1982). Preliminary ultrastructural and autoradiographic evidence that the trophonema of the sea anemone *Actinia fragacea* has a nutritive function. Int. J. Invertebr. Reprod. *4*, 375–379.

45. Levitan, S., Sher, N., Brekhman, V., Ziv, T., Lubzens, E., and Lotan, T. (2015). The making of an embryo in a basal metazoan: proteomic analysis in the sea anemone *Nematostella vectensis*. Proteomics *15*, 4096–4104.

46. Shikina, S., Chen, C.J., Chung, Y.J., Shao, Z.F., Liou, J.Y., Tseng, H.P., Lee, Y.H., and Chang, C.F. (2013). Yolk formation in a stony coral *Euphyllia ancora* (Cnidaria, Anthozoa): insight into the evolution of vitellogenesis in nonbilaterian animals. Endocrinology *154*, 3447–3459.

47. Shikina, S., Chiu, Y.L., Lee, Y.H., and Chang, C.F. (2015). From somatic cells to oocytes: a novel yolk protein produced by ovarian somatic cells in a stony coral, Euphyllia ancora. Biol. Reprod. *93*, 57.

48. Tan, E.S., Izumi, R., Takeuchi, Y., Isomura, N., and Takemura, A. (2020). Molecular approaches underlying the oogenic cycle of the scleractinian coral, *Acropora tenuis*. Sci. Rep. *10*, 9914.

49. Lotan, T., Chalifa-Caspi, V., Ziv, T., Brekhman, V., Gordon, M.M., Admon, A., and Lubzens, E. (2014). Evolutionary conservation of the mature oocyte proteome. EuPA Open Proteom. *3*, 27–36.

50. Eckelbarger, K.J., Tyler, P.A., and Langton, R.W. (1998). Gonadal morphology and gametogenesis in the sea pen *Pennatula aculeata* (Anthozoa: Pennatulacea) from the Gulf of Maine. Mar. Biol. *132*, 677–690.

51. Schneider, W.J. (1996). Vitellogenin receptors: oocyte-specific members of the low-density lipoprotein receptor supergene family. Int. Rev. Cytol. *166*, 103–137.

52. Voet, D., Voet, J., and Pratt, C.W. (2016). Fundamentals of Biochemistry: Life at the Molecular Level (Wiley).

53. Wourms, J.P. (1987). Oogenesis. In Reproduction of Marine Invertebrates, Volume IX, General Aspects: Seeking Unity in Diversity, A.C. Giese, J.S. Pearse, and V.B. Pearse, eds. (Blackwell Scientific Publications), pp. 50–157.

54. K.G. Adiyodi, and R.G. Adiyodi, eds. (1983). Reproductive Biology of Invertebrates, Volume I: Oogenesis, Oviposition, and Oosorption (John Wiley & Sons).

55. Yonge, C.M., and Nicholls, A.G. (1930). The structure, distribution and physiology of the Zooxanthellae. In Studies on the Physiology of Corals (British Museum), pp. 136–176.

56. Krasity, B.C., Troll, J.V., Weiss, J.P., and McFall-Ngai, M.J. (2011). LBP/BPI proteins and their relatives: conservation over evolution and roles in mutualism. Biochem. Soc. Trans. *39*, 1039–1044.

57. Gazi, U., and Martinez-Pomares, L. (2009). Influence of the mannose receptor in host immune responses. Immunobiology *214*, 554–561.

58. Gumienny, T.L., Brugnera, E., Tosello-Trampont, A.C., Kinchen, J.M., Haney, L.B., Nishiwaki, K., Walk, S.F., Nemergut, M.E., Macara, I.G., Francis, R., et al. (2001). CED-12/ELMO, a novel member of the CrkII/Dock180/Rac pathway, is required for phagocytosis and cell migration. Cell *107*, 27–41.

59. Broderick, N.A. (2015). A common origin for immunity and digestion. Front. Immunol. *6*, 72.

60. Wang, J., Sun, H., Jiang, M., Li, J., Zhang, P., Chen, H., Mei, Y., Fei, L., Lai, S., Han, X., et al. (2021). Tracing cell-type evolution by cross-species comparison of cell atlases. Cell Rep. *34*, 108803.

61. Pedersen, K.J. (1961). Studies on the nature of planarian connective tissue. Zeitschrift für Zellforschung *53*, 569–608.

62. Prummel, K.D., Nieuwenhuize, S., and Mosimann, C. (2020). The lateral plate mesoderm. Development *147*, dev175059.

63. Huang, L.S., Voyiaziakis, E., Chen, H.L., Rubin, E.M., and Gordon, J.W. (1996). A novel functional role for apolipoprotein B in male infertility in heterozygous apolipoprotein B knockout mice. Proc. Natl. Acad. Sci. USA *93*, 10903–10907.

64. Huang, L.S., Voyiaziakis, E., Markenson, D.F., Sokol, K.A., Hayek, T., and Breslow, J.L. (1995). apo B gene knockout in mice results in embryonic lethality in homozygotes and neural tube defects, male infertility, and reduced HDL cholesterol ester and apo A-I transport rates in heterozygotes. J. Clin. Invest. *96*, 2152–2161.

65. Young, J.A.C. (1974). The nature of tissue regeneration after wounding in the sea anemone Calliactis Parasitica (Couch). J. Mar. Biol. Ass. *54*, 599–617.

66. Van-Praët, M. (1978). Étude histochimique et ultrastructurale des zones digestives d'*Actinia equina L.* (Cnidaria, Actinaria). Cah. Biol. Mar. *XIX*, 415–432.

67. Larkman, A.U. (1984). The fine structure of granular amoebocytes from the gonads of the sea anemone *Actinia fragacea* (Cnidaria: Anthozoa). Protoplasma *122*, 203–221.

68. Putnam, N.H., Srivastava, M., Hellsten, U., Dirks, B., Chapman, J., Salamov, A., Terry, A., Shapiro, H., Lindquist, E., Kapitonov, V.V., et al. (2007). Sea anemone genome reveals ancestral eumetazoan gene repertoire and genomic organization. Science *317*, 86–94.

69. Fredman, D., Schwaiger, M., Rentzsch, F., and Technau, U. (2013). Nematostella vectensis transcriptome and gene models v2.0. Dataset. https://doi.org/10.6084/m9.figshare.807696.v3.

70. Levy, S., Elek, A., Grau-Bové, X., Menéndez-Bravo, S., Iglesias, M., Tanay, A., Mass, T., and Sebé-Pedrós, A. (2021). A stony coral cell atlas illuminates the molecular and cellular basis of coral symbiosis, calcification, and immunity. Cell *184*, 2973–2987.e18.

71. Sebé-Pedrós, A., Chomsky, E., Pang, K., Lara-Astiaso, D., Gaiti, F., Mukamel, Z., Amit, I., Hejnol, A., Degnan, B.M., and Tanay, A. (2018). Early metazoan cell type diversity and the evolution of multicellular gene regulation. Nat. Ecol. Evol. *2*, 1176–1188.

72. Fincher, C.T., Wurtzel, O., de Hoog, T., Kravarik, K.M., and Reddien, P.W. (2018). Cell type transcriptome atlas for the planarian *Schmidtea mediterranea*. Science *360*, eaaq1736.

73. Plass, M., Solana, J., Wolf, F.A., Ayoub, S., Misios, A., Glažar, P., Obermayer, B., Theis, F.J., Kocks, C., and Rajewsky, N. (2018). Cell type atlas and lineage tree of a whole complex animal by single-cell transcriptomics. Science *360*, aaq1723.

74. Edgar, R.C. (2004). MUSCLE: multiple sequence alignment with high accuracy and high throughput. Nucleic Acids Res. *32*, 1792–1797.

75. Castresana, J. (2000). Selection of conserved blocks from multiple alignments for their use in phylogenetic analysis. Mol. Biol. Evol. *17*, 540–552.

76. Trifinopoulos, J., Nguyen, L.T., von Haeseler, A., and Minh, B.Q. (2016). W-IQ-TREE: a fast online phylogenetic tool for maximum likelihood analysis. Nucleic Acids Res. *44*, W232–W235.

77. Ronquist, F., and Huelsenbeck, J.P. (2003). MrBayes 3: Bayesian phylogenetic inference under mixed models. Bioinformatics *19*, 1572–1574.

78. Untergasser, A., Nijveen, H., Rao, X., Bisseling, T., Geurts, R., and Leunissen, J.A.M. (2007). Primer3Plus, an enhanced web interface to Primer3. Nucleic Acids Res. *35*, W71–W74.

79. Concordet, J.P., and Haeussler, M. (2018). CRISPOR: intuitive guide selection for CRISPR/Cas9 genome editing experiments and screens. Nucleic Acids Res. *46*, W242–W245.

80. Schindelin, J., Arganda-Carreras, I., Frise, E., Kaynig, V., Longair, M., Pietzsch, T., Preibisch, S., Rueden, C., Saalfeld, S., Schmid, B., et al. (2012). Fiji: an open-source platform for biological-image analysis. Nat. Methods *9*, 676–682.

81. Hand, C., and Uhlinger, K.R. (1992). The culture, sexual and asexual reproduction, and growth of the sea anemone *Nematostella vectensis*. Biol. Bull. *182*, 169–176.

82. Fritzenwanker, J.H., and Technau, U. (2002). Induction of gametogenesis in the basal cnidarian *Nematostella vectensis* (Anthozoa). Dev. Genes Evol. *212*, 99–103.

83. Zimmermann, B., Robb, S.M.C., Genikhovich, G., Fropf, W.J., Weilguny, L., He, S., Chen, S., Lovegrove-Walsh, J., Hill, E.M., Ragkousi, K., et al. (2020). Sea anemone genomes reveal ancestral metazoan chromosomal macrosynteny. Preprint at bioRxiv. https://doi.org/10.1101/2020.10.30.359448.

84. Ronquist, F., Teslenko, M., van der Mark, P., Ayres, D.L., Darling, A., Höhna, S., Larget, B., Liu, L., Suchard, M.A., and Huelsenbeck, J.P. (2012). MrBayes 3.2: efficient Bayesian phylogenetic inference and model choice across a large model space. Syst. Biol. *61*, 539–542.

85. Altekar, G., Dwarkadas, S., Huelsenbeck, J.P., and Ronquist, F. (2004). Parallel metropolis coupled Markov chain Monte Carlo for Bayesian phylogenetic inference. Bioinformatics *20*, 407–415.

86. Genikhovich, G., and Technau, U. (2009). In situ hybridization of starlet sea anemone (*Nematostella vectensis*) embryos, larvae, and polyps. Cold Spring Harb. Protoc. *2009*. pdb.prot5282.

87. Sinigaglia, C., Thiel, D., Hejnol, A., Houliston, E., and Leclère, L. (2018). A safer, urea-based in situ hybridization method improves detection of gene expression in diverse animal species. Dev. Biol. *434*, 15–23.

88. Bassett, A.R., Tibbit, C., Ponting, C.P., and Liu, J.L. (2013). Highly efficient targeted mutagenesis of *Drosophila* with the CRISPR/Cas9 system. Cell Rep. *4*, 220–228.

89. Subach, O.M., Patterson, G.H., Ting, L.M., Wang, Y., Condeelis, J.S., and Verkhusha, V.V. (2011). A photoswitchable orange-to-far-red fluorescent protein, PSmOrange. Nat. Methods *8*, 771–777.

90. Gibson, D.G., Young, L., Chuang, R.Y., Venter, J.C., Hutchison, C.A., and Smith, H.O. (2009). Enzymatic assembly of DNA molecules up to several hundred kilobases. Nat. Methods *6*, 343–345.

91. Gutierrez-Triana, J.A., Tavhelidse, T., Thumberger, T., Thomas, I., Wittbrodt, B., Kellner, T., Anlas, K., Tsingos, E., and Wittbrodt, J. (2018). Efficient single-copy HDR by 5′ modified long dsDNA donors. eLife *7*, 1–15.

92. Kraus, Y., Aman, A., Technau, U., and Genikhovich, G. (2016). Pre-bilaterian origin of the blastoporal axial organizer. Nat. Commun. *7*, 11694.

93. Burger, A., Lindsay, H., Felker, A., Hess, C., Anders, C., Chiavacci, E., Zaugg, J., Weber, L.M., Catena, R., Jinek, M., et al. (2016). Maximizing mutagenesis with solubilized CRISPR-Cas9 ribonucleoprotein complexes. Development *143*, 2025–2037.

94. Schlombs, K., Wagner, T., and Scheel, J. (2003). Site-1 protease is required for cartilage development in zebrafish. Proc. Natl. Acad. Sci. USA *100*, 14024–14029.

95. O'Rourke, E.J., Soukas, A.A., Carr, C.E., and Ruvkun, G. (2009). *C. elegans* major fats are stored in vesicles distinct from lysosome-related organelles. Cell Metab. *10*, 430–435.

STAR★METHODS

KEY RESOURCES TABLE

REAGENT or RESOURCE	SOURCE	IDENTIFIER
Antibodies		
Rabbit anti-DsRed	Takara/Clontech	Cat#632496; RRID: AB_10013483
Secondary goat anti-Rabbit IgG (H+L) coupled with Alexa Fluor 568	Life Tech	Cat#A11011; RRID: AB_143157
Biological samples		
ApoB-PSmOrange transgenic line	This study	N/A
Critical commercial assays		
FluoSpheres Carboxylate-modified microspheres, 1μm, crimson fluorescent (625/645)	Invitrogen	Cat#F8816
FluoSpheres Carboxylate-modified microspheres, 20nm, yellow-green fluorescent (505/515)	Invitrogen	Cat#F8787
Escherichia coli (K-12 strain) BioParticles, Alexa Fluor 488 conjugate	Invitrogen	Cat#E13231
Oleic acid(17-yne), ethanol solution	Avanti Polar Lipids	Cat#900412E
Click-iT EdU Cell Proliferation Kit	Invitrogen	Cat#C10337
Alexa Fluor 488 Azide	Invitrogen	Cat#A10266
Deposited data		
Nematostella vectensis genome	Putnam et al.[68]	https://mycocosm.jgi.doe.gov/Nemve1/Nemve1.home.html
Nematostella vectensis egg proteome	Lotan et al.[49]	N/A
Nematostella vectensis transcriptome	Fredman et al.[69]	https://mycocosm.jgi.doe.gov/Nemve1/Nemve1.home.html
Nematostella vectensis single-cell transcriptome	Sebé-Pedrós et al.[35]	N/A
Stylophora pistillata single-cell transcriptome	Levy et al.[70]	https://sebe-lab.shinyapps.io/Stylophora_cell_atlas/
Amphimedon queenslandica single-cell transcriptome	Sebé-Pedrós et al.[71]	N/A
Schmidtea mediterranea single-cell transcriptomes	Fincher et al.[72] and Plass et al.[73]	https://digiworm.wi.mit.edu/; https://shiny.mdc-berlin.de/psca/
cDNA fragments cloned for ISH	This study	Deposited to Genbank, accession # in Data S2
Experimental models: Organisms/strains		
Nematostella vectensis	Sars Centre	N/A
Nematostella: *apoB*-PSmOrange fusion protein transgenic reporter line	This study	N/A
Oligonucleotides		
Primers for ISH gene cloning, gRNA oligos and primers for PCR and sequencing of the ApoB transgenic lines can be found in Data S2	This study	N/A
Recombinant DNA		
pH2B-PSmOrange	Gifted by Vladislav Verkhusha	Addgene plasmid #31920[4]
Plasmid: apoB-PSmOrange (pJet1.2 backbone)	This study	N/A
Software and algorithms		
MUSCLE v3.8.31	Edgar[74]	https://www.drive5.com/muscle/
GBlocks	Castresana[75]	http://molevol.cmima.csic.es/castresana/Gblocks.html

(*Continued on next page*)

Continued

REAGENT or RESOURCE	SOURCE	IDENTIFIER
iqTree	Trifinopoulos et al.[76]	http://iqtree.cibiv.univie.ac.at/
MrBayes v3.2.7	Ronquist and Huelsenbeck[77]	https://nbisweden.github.io/MrBayes/
FigTree v1.4.4	N/A	https://github.com/rambaut/figtree/releases
Primer3Plus	Untergasser et al.[78]	http://www.bioinformatics.nl/cgi-bin/primer3plus/primer3plus.cgi
CRISPOR	Concordet and Haeussler[79]	http://crispor.tefor.net/
Fiji	Schindelin et al.[80]	https://imagej.net/software/fiji/

RESOURCE AVAILABILITY

Lead contact

Further information and requests for resources and reagents should be directed to and will be fulfilled by the lead contact, Patrick R. H. Steinmetz (patrick.steinmetz@uib.no).

Materials availability

Plasmids and genetically modified *Nematostella vectensis* generated for this study are available upon completion of a Material Transfer Agreement.

Data and code availability

cDNA fragments amplified and cloned for generating *in situ* hybridization probes have been deposited in Genbank and are publicly available as of the date of publication. Accession numbers are listed in Data S2. This paper does not report original code. Any additional information required to reanalyze the data reported in this paper is available from the lead contact upon request.

EXPERIMENTAL MODEL AND SUBJECT DETAILS

Nematostella vectensis culture

Nematostella vectensis polyps are derived from the original culture established by C. Hand and K. Uhlinger.[81] Adult animals (> 6 months) were maintained in the dark at 18°C in 16ppm diluted sea water (*Nematostella* medium, NM) and fed 5 days per week with brine shrimp nauplii. Spawning was induced approximately every three weeks by a 12-hours shift in temperature (from 18°C to 25°C) and exposure to light, as described previously.[82] For injection, fertilized egg packages were incubated in a 3% (w/v) cysteine/NM solution to remove the egg jelly. Injected animals were raised at 25°C for 2 to 3 months, and subsequently transferred to 18°C for regular induction. The use of female or male specimen is specified in the figures and figure legends throughout the manuscript wherever relevant.

METHOD DETAILS

Particle uptake assays and tissue fixation

Fluorescent latex beads (FluoSpheres, FS) of 1μm (Thermo Fischer, carboxylate-modified, crimson fluorescent, Ex/Em = 625/645) and 20nm diameter (Thermo Fisher, carboxylate-modified, yellow-green fluorescent, Ex/Em = 505/515) were incubated for 2 hours in 2% (w/v) Bovine Serum Albumine (BSA)/NM solution at a 1:1 ratio and further diluted 1:100 in 0.1M MgCl2/NM before use.

For the bacteria uptake assay, *E. coli* K-12 strain Bioparticles (Thermo Fisher, Alexa Fluor 488 conjugate, Ex/Em = 495/519) were resuspended in filtered water to reach a stock concentration of $3x10^8$ particles/ml and further diluted 1:100 in 0.1M $MgCl_2$/NM to $3x10^6$ particles/ml before use.

For all particle uptake assays, animals were initially relaxed in 0.1M $MgCl_2$/NM for 20 minutes and were kept in this medium for incubation times below 4 hours. For longer incubations, animals were kept in $MgCl_2$/NM for the first 4 hours and then transferred to fresh NM. The diluted Fluospheres or *E. coli* solution was injected inside the body cavity through the mouth using a thinned glass Pasteur pipet. The animals were kept in the dark at 18°C during incubation.

At the end of the assays, animals kept in NM were transferred back to 0.1M $MgCl_2$/NM solution and left to relax for 20 minutes. The body cavity of all animals was flushed and inflated with this medium through the mouth to ensure full extension of the mesenteries. The polyps were then transferred to a 3.7% (v/v) Formaldehyde (Merck)/NM solution and opened longitudinally along the body column to ensure penetrance of the fixative and to allow non-internalized particles to be washed off. Polyps were fixed overnight at 4°C in the dark, after which the mesenteries were dissected in fixative and cut to 3-5mm long pieces. The tissue pieces were washed in 1x PBS/0.1% (v/v) Tween-20, counterstained for F-actin with Phalloidin (1:17, Alexa-488 or Alexa-647; Thermo Fisher) and DAPI nuclear staining (1:1000) before being processed for cryosectioning.

Candidate gene identification and orthology, single-cell datasets comparison

Candidate genes were identified using a literature search that included a published *N. vectensis* egg proteome,[49] transcriptome[35,69] datasets as well as BLAST of the publicly available genome.[68,83] Orthology was confirmed by reciprocal BLASTP using the NCBI BLAST platform (http://www.ncbi.nlm.nih.gov/blast/) and phylogenetic analyses. We used the published single-cell transcriptomes of *Nematostella*,[35] *S. pistillata*,[70] *A. queenslandica*[71] and *S. mediterranea*[72,73] as resources for gene expression profile comparisons.

Phylogeny

Amino acid sequences were retrieved using the NCBI BLAST platform and aligned using MUSCLE v3.8.31.[74] Sequence stripping was performed with GBlocks[75] using the least conservative parameters (Min. Num. of Seq. for Flank Pos: lowest possible; Min. Block Length: 2; Gaps set to "half"). Stripped alignments were tested for the best fitting maximum likelihood parameters (LDLR, LRP1: WAG+I+G4; Vtg: LG+I+G4) and maximum likelihood trees calculated with iqTree using ultrafast bootstrapping (1000 replicates). Bayesian posterior probabilities were calculated using MrBayes v3.2.7[77,84,85] using LG+I+G8 (Vtg) or WAG+I+G4 (LDLR, LRP1) model parameters, two parallel runs, a temperature of 0.2 (LDLR, LRP1) or 0.05 (Vtg), eight chains, 1 (LDLR, LPR1) or 2 (Vtg) swaps tried at each swapping generation, and a sample frequency of every 10 generations. Convergence was reached after 20.000 (LDLR), 80.000 (Vtg) or 100.000 (LPR1) generations. A consensus tree was calculated using a burn-in of 5000 generations. Maximum-likelihood phylogenetic analyses were run on the IQ-TREE web server (http://iqtree.cibiv.univie.ac.at/; Trifinopoulos et al.[76]) using the best-fit substitution model and an ultrafast bootstrap analysis with 1000 alignments. Trees were visualized using FigTree v1.4.4 (https://github.com/rambaut/figtree/releases) and modified using Adobe Illustrator 2022 for MacOS.

Gene cloning and RNA probe synthesis

RNA was extracted from whole adult female *Nematostella* polyps using Trizol (Thermo Fisher), following the manufacturer's protocol. cDNA was obtained using the SuperScript III first-strand synthesis system (Thermo Fisher). Fragments of the genes of interest were amplified using primers designed with the Primer3Plus online tool[78] (http://www.bioinformatics.nl/cgi-bin/primer3plus/primer3plus.cgi). The fragments were then inserted in a pGEM-T Easy vector (Promega) and transformed into One Shot Top 10 chemically competent *E. coli* (Invitrogen). Cloned sequences were verified by Sanger sequencing at the sequencing facility of the Department of Biological Sciences, University of Bergen, Bergen, Norway. Antisense RNA probes were generated using a T7 or SP6 MEGAscript Kit (Invitrogen) and labelled with Digoxygenin (DIG) RNA Labelling Mix (Roche) according to the manufacturers' protocols (see also Genikhovich and Technau[86]). Gene accession numbers for all cloned genes are listed in Data S2.

In situ hybridization

Adult polyps were fixed as described above (see particle uptake assays and tissue fixation). Dissected pieces of mesenteries were washed up to 5 times over a period of 30-90 minutes in 100% methanol until all pigmentation was removed and stored in 100% methanol at -20°C.

The urea-based *in situ* hybridization protocol was adapted from a previously published protocol.[87] All steps are conducted in mesh sieves under gentle rotation except for Proteinase K digestion (no rotation). After progressive rehydration from 100% MeOH to 100% PTx (0.3% (v/v) Triton X-100 in 1xPBS pH 7.4), the tissue was digested with 2.5μg/ml Proteinase K in PTx for 5 minutes at room temperature (RT). Enzymatic digestion is stopped by two washes in 2mg/ml glycine/PTx. Samples were then washed in 1% (v/v) triethanolamine (TEA) in PTx, followed by a 1%TEA/ 3μg/ml acetic anhydride and a 1%TEA/6μg/ml acetic anhydride washing steps. After two PTx washes, tissue pieces were post-fixed for 2 min in 0.2% (v/v) glutaraldehyde/PTx and 1 hour in 3.7% formaldehyde (FA, v/v)/PTx. After washes in PTx and hybridization buffer (HB: 50% (v/v) 8M urea, 5x SSC pH 4.5, 0.3% (v/v) Triton X-100, 1% (w/v) SDS, 100 μg/ml heparin, 5 mg/ml Torula yeast RNA), we performed an overnight blocking step at 60°C in blocking buffer (5% (w/v) dextran sulfate (MW > 500,000, Sigma-Aldrich), 3% (w/v) Blocking Reagent (Roche) in HB). On the next day, digoxigenin (DIG)-labelled probes (see Gene cloning and RNA probe synthesis) were diluted to 0.75ng/μl in blocking buffer and denatured for 10 minutes at 80°C before addition to the samples. Hybridization was conducted at 60°C over two days. Unbound probe was removed via a series of 60°C washes in HB/2X SSCT (0.03M sodium citrate, 0.3M NaCl, 0.3% (v/v) Triton X-100) solutions [75/25, 50/50, 25/75, 0/100 (v/v)] and in 0.1X SSCT. Additional washes in 0.1X SSCT/PTx were performed at RT [66/33, 33/66, 0/100 (v/v)], followed by consecutive washes in PBTx (0.1% (w/v) BSA, 0.3% (v/v) Triton X-100 in 1X PBS). Samples were then blocked for 1 hour in blocking solution (1% (w/v) Blocking Reagent (Roche)/maleic acid buffer (150mM maleic acid, 100mM NaCl, pH=7.5)) and incubated overnight with 1:2000 anti-DIG alkaline phosphatase antibody (Roche)/blocking solution (preabsorbed for 1h). On the next day, unbound antibody was removed by 10 increasingly long washes (2-30 minutes over a period of 2h30) with PBTx, after which samples were washed with alkaline phosphatase buffer (AP: 100mM NaCl, 50mM $MgCl_2$, 100mM Tris pH9.5, 0.1% (v/v) Tween-20). The staining reaction (4.5μl/ml NBT, 3.5μl/ml BCIP in AP buffer) was performed at RT for 5 minutes (strongly expressed genes) to 8 hours (weakly expressed genes). The reaction was stopped by washing in PTw (0.1% (v/v) Tween-20 in 1X PBS), and unspecific staining removed by a 2 minutes 100% ethanol wash. Staining quality was further improved by storing the samples in 87% glycerol at 4°C for several days before further processing.

Alkyne-oleic acid assays and Click-it reaction

Stock solution of alkyne-modified oleic acid (17-yne) (alkyne-OA, Avanti Polar Lipids, ethanol solution 1mg/ml) was aliquoted, and the ethanol evaporated in a vacuum concentrator.

For pulse-chase experiments in Figures 3A–3E and S3D–S3H, alkyne-OA was resuspended in DMSO to 3mg/ml, and further diluted to a final concentration of 0.3mg/ml in NM containing freshly hatched *Artemia salina* nauplii. Artemia were incubated in this solution for 2 hours, washed several times with NM on a fine mesh filter and resuspended in NM. Adult *Nematostella* polyps fasted overnight were each fed a few drops of enriched artemia and left to catch and ingest the prey for 4 hours. They were placed in clean medium after the feeding period and fixed after 20 hours or 7 days chase periods. During the 7 days chase period, animals were fed 5x/week with regular nauplii.

Alkyne-OA/BSA assays in Figures 3F–3J and S3I–S3N were performed with alkyne-OA directly resuspended in a 4 mg/ml fatty acid-free BSA/NM solution following the manufacturer's protocol. Overnight-fasted adult *Nematostella* polyps were relaxed in 0.1M $MgCl_2$/NM for 20 minutes before alkyne-OA/BSA solution was injected into the gastric cavity through the mouth using a thinned Pasteur pipet.

Animals kept in NM were transferred to 0.1M $MgCl_2$/NM solution and left to relax for 20 minutes prior to fixation, while animals that had been incubated in $MgCl_2$ during the assay were processed directly. Fixation was conducted following the same protocol as described above (see particle uptake assays and tissue fixation). Fixation took place 30 minutes, 1 hour or 2 hours after alkyne-OA exposure, or after the chase.

Alkyne-modified oleic acid was visualized in the tissue by performing a click chemistry reaction using an azide-modified fluorophore (Alexa Fluor 488 Azide, Invitrogen, Ex/Em = 495/519). Fixed tissue pieces were blocked for 30 minutes at 4°C in a 3% (w/v) BSA/1x PBS solution, followed by a 30 minutes permeabilization step at 4°C in PTx. The click reaction was performed using the reagents of a Click-iT EdU Cell Proliferation Kit for Imaging (Invitrogen) following the manufacturer's protocol. The staining reaction was conducted for 30 minutes at room temperature. The tissue was then washed in 1x PBS three times over a period of 2 hours to remove unbound fluorophore and stained with DAPI nuclear staining before cryosection.

CRISPR-Cas9 mediated generation of ApoB-PSmOrange knock-in line

Two guide RNA (gRNA) target regions with predicted cutting sites located 52bp upstream or 24bp downstream of the Stop codon of the *Nematostella apoB* gene (v1g84136/NVE25290) were designed using CRISPOR.[79] Templates for gRNAs were generated using annealed and PCR-amplified oligos:[88] two T7- and gRNA-encoding oligos (Thermo Fisher, desalted): 5′-GAAATTAATACGACTCAC TATAG**TCCTGTGTACATGGATACGT**GTTTTAGAGCTAGAAATAGCAAG-3′ (upstream of Stop codon); 5′- GAAATTAATACGACT CACTATAG**actaatcctaattaccaagt**GTTTTAGAGCTAGAAATAGCAAG-3' (downstream of Stop codon) and an invariant reverse primer (Thermo Fisher, desalted): 5'-AAAAGCACCGACTCGGTGCCACTTTTTCAAGTTG ATAACGGACTAGCCTTATTTTAACTTGC TATTTCTAGCTCTAAAAC-3'.

Guide RNAs were *in vitro* transcribed using a T7 MegaScript transcription kit (Thermo Fisher) followed by ammonium chloride precipitation and resuspended in nuclease-free H_2O to a final concentration of 1.5μg/μl. The DNA donor fragment for homology-mediated repair (HDR) consisted of a $(GGGGS)_2$ linker and a PSmOrange ORF cloned in frame to the 3' end of the *apoB* ORF, and framed by a 1030bp long 'left' and a 973bp 'right' homology arm. pH2B-PSmOrange was a gift from Vladislav Verkhusha (Addgene plasmid #31920; Subach et al.[89]). The entire construct was cloned into a pJet1.2 plasmid backbone (Thermo Fisher) using Gibson assembly (NEB Master mix).[90] Donor DNA fragment was PCR-amplified using 5′-biotin-labelled oligos flanking the donor fragment to increase integration efficiency as previously described.[91] Oligo sequences (Thermo Fisher; desalted) were: Forward oligo 5'-[Biotin]-TAC-GACTCACTATAGGGAGAGCGGC-3'; reverse oligo 5'-[Biotin]-CCATGGCAGCTGAGAATATTGTAGGA-3'.

The Cas9-mediated knock-in injection was performed by modifying previously described protocols for CRISPR/Cas9-mediated mutagenesis and used 0.75μg/μl nls-Cas9 protein (PacBio), 75ng/μl of each guide RNA, 70ng/μl column-purified donor DNA, and modified injection buffer containing 220mM KCl.[92,93] Out of approx. 2300 injected zygotes, one single ubiquitously fluorescent polyp was identified and raised as founder animal. The success of the knock-in has been validated on the transcript level by *in vitro* synthesis of cDNA based on extracted total RNA from a mix of fluorescent F1 juvenile polyps. Based on this cDNA, the transitions between the apoB ORF and PSmOrange, and between PSmOrange and the 3'UTR have been amplified using oligos flanking the 'homology arm' regions. Sanger sequencing of gel-eluted and column-purified PCR fragments confirmed the flawless integration of the $(GGGGS)_2$-PSmOrange fragment directly downstream of the *apoB* open reading frame. Oligos used for PCR & sequencing: ApoB-Forward : 5'- GACTGCTAAGGACATGAAGCACTGC-3'; ApoB-Reverse (not used for sequencing): 5' GACTTCGTCATACTCCGATA CTGGAC -3'; PSmOrange-Forward (used with ApoB-Reverse): 5'- CAACGAGGACTACACCATCGTGG-3'; PSmOrange-Reverse (used with ApoB-Forward): 5'-CTCGAACTCGTGGCCGTTCAC-3'. Additional sequencing oligo: ApoB-Reverse-2: AATCATAGC ACCACCTCACTGCG.

Immunofluorescence

Animals were fixed overnight and dissected in fixative (3.7% FA, 0.5% DMSO, 0.1% Tween20/1x PBS pH 7.4 (v/v)), then stored in 100% methanol at -20°C before use. After progressive rehydration in 1xPBS, tissue pieces were incubated in blocking buffer (5% (v/v) NGS, 1% (w/v) BSA, 0.2% (v/v) Triton X-100/1x PBS) for 30 minutes at room temperature. They were then incubated with pre-absorbed primary antibody (rabbit anti-DsRed/blocking buffer, 1:100, Takara Bio Clontech) overnight at 4°C. On the next day, the tissue was washed 6x with PTx, blocked again (see above), and incubated with pre-absorbed secondary antibody (goat-anti-rabbit-Alexa568/blocking buffer, 1:1000, LifeTech). Finally, tissue pieces were washed several times and overnight in PTx, stained with DAPI nuclear staining and processed for cryosectioning.

Cryotome sectioning

After overnight infiltration in 25% (w/v) sucrose, 20% (v/v) OCT (Tissue-Tek O.C.T. Compound, Sakura)/1x PBS, samples were mounted in 80% (v/v) OCT/1x PBS, oriented for transversal sections and frozen on a metal block cooled with liquid N_2. Sectioning was performed at −25°C in a Leica Cryostat CM1850 and the 12μm sections were mounted on Thermo Scientific SuperFrost Plus adhesion slides (Thermo Fisher). After drying, the sections were post-fixed for 10 min in 3.7% (v/v) FA/1x PBS, rinsed 2x in 1xPBS, and mounted in 87% glycerol (non-fluorescent samples) or ProLong Gold antifade reagent (Molecular Probes, fluorescent samples).

Oil Red O staining

Animals were fixed, dissected and mesentery pieces sectioned with a cryotome and post-fixed as described above. Oil Red O (ORO) stock solution was prepared by diluting 5mg/ml ORO powder in isopropanol, shaking at room temperature for 4 hours. The stock solution was further diluted to 60% (v/v) in milliQ water, left shaking at room temperature for another 2 hours and filtered using a 0.22μm syringe filter to produce a working solution.[94,95] Glass slides with mesentery sections were incubated for 15 minutes with the ORO working solution, then washed several times in 1xPBS.

Transmitted light and confocal imaging

Images of *in situ* hybridization- and ORO-stained tissue were taken on a Nikon Eclipse E800 using a 20x air, 40x air or 60x oil-immersion objective. Images of fluorescent assays were taken either on a Leica SP5 confocal microscope using standard PMT detectors and a 20x or 63x oil-immersion lens, on a Leica SP8 confocal microscope using HyD detectors and 40x water-immersion or 100x oil-immersion objectives, or on an Olympus FLUOVIEW FV3000 confocal microscope using standard PMT detectors and a 60x silicon oil immersion lens. Transmitted light images were corrected for levels and colour balance and cropped using Photoshop CC. Fluorescent stacks were processed, cropped and the levels corrected using Fiji.[80]